Photodiagnosis and Photodynamic Therapy 33 (2021) 102190

Contents lists available at ScienceDirect

Photodiagnosis and Photodynamic Therapy

journal homepage: www.elsevier.com/locate/pdpdt

Delineation of the Arm Blood Vessels Utilizing Hyperspectral Imaging to Assist with Phlebotomy for Exploiting the Cutaneous Tissue Oxygen Concentration

Mohamed Hisham Fouad Aref [a,*], Amr A.R. Sharawi [b], Yasser H. El-Sharkawy [c]

[a] Biomedical Engineering Department, Military Technical College, Cairo, Egypt
[b] Systems and Biomedical Engineering Department, Cairo University, Faculty of Engineering, Egypt
[c] Head of Biomedical Engineering Department, Military Technical College, Cairo, Egypt

ARTICLE INFO

Keywords:
Blood Vessels Viewer
Hyperspectral Imaging system
Oxygen Saturation
K-mean Clustering Algorithm
Remote Sensing

ABSTRACT

Significance: The estimation of tissue oxygenation is vital in the diagnosis and therapeutic evaluation of a huge assortment of diseases. The hyperspectral (HS) imaging system is a rising innovation that can be utilized to build a highly sensitive, non-invasive, and tissue hemoglobin immersion map.
Objective: As a result of the urgent need to design and implement early detection devices and applications for the COVID-19 pandemic, we propose building a non-invasive custom optical imaging system to assist with phlebotomy and vascular approach to survey the reliability of blood oxygen saturation (SpO2) levels recovered from spectral images.
Materials and Methods: HS images were gathered from 15 healthy subjects without previous medical history complications and with an average age range of 20 to 38 years, who were undergoing phlebotomy. The forearm was vigorously illuminated utilizing an HS camera with polychromatic source light of spectrum range (400∼980 nm). Spectroscopic reflectance images were caught by a focal plane exhibit for the region of interest (ROI). Then the custom algorithm comprising normalization and moving average filtering for noise removal was applied, followed by K-mean clustering for image segmentation to visualize and highlight the arteries and the veins in the investigated forearm.
Results: The investigations show that after normalization of the recorded signal from the HS camera of the participating subjects it was noticed that at wavelength of 460 nm the oxygenated arteries had a stronger signal than the de-oxygenated veins, and at a wavelength of 750 nm the de-oxygenated veins had a stronger signal than the oxygenated arteries. Thus, the ideal wavelength to reveal the oxygenated arteries was 460 nm, and the ideal wavelength to reveal the de-oxygenated veins was 750 nm.
Conclusions: HSI is a prospective technique to assist with phlebotomy and non-contact oxygen saturation approach. Additionally, it may permit future surgical or pharmacological intercessions that titrate or limit ischemic injury continuously.

1. Introduction

The degree of blood oxygenation in specific zones of the body relies upon numerous elements like pneumonic hemostasis, local and systemic blood circulation. Therefore, the measurement of blood oxygenation can bring data concerning all the previously mentioned physiological functions [1]. The oxygen saturation in the blood (SpO2) is a significant factor for clinical diagnosis, which gives important data to the conventional treatment of a few neurotic conditions such as hypoxemia, sepsis, or decompression sickness [2].

The degree of the oxygen level in the blood with high accuracy can be exploited as an observing parameter for cardiac and respiratory system illness and additionally, in the assessment of vascular diseases such as: diabetic ulcers in the foot, plastic surgeries, and burned skin [1]. Microcirculation is vital for the biological tissue`s source of oxygen and nutritive substances and the expulsion of waste outcomes [3].

Different strategies have been created for direct or indirect assurance of tissue oxygenation and are currently utilized in both clinical practice

* Corresponding author at: Building (3), Block No (7078), El-Mokattam, 11571, Cairo, Egypt.
E-mail address: MH-Aref@ieee.org (M.H. Fouad Aref).

https://doi.org/10.1016/j.pdpdt.2021.102190
Received 14 November 2020; Received in revised form 1 January 2021; Accepted 15 January 2021
Available online 26 January 2021

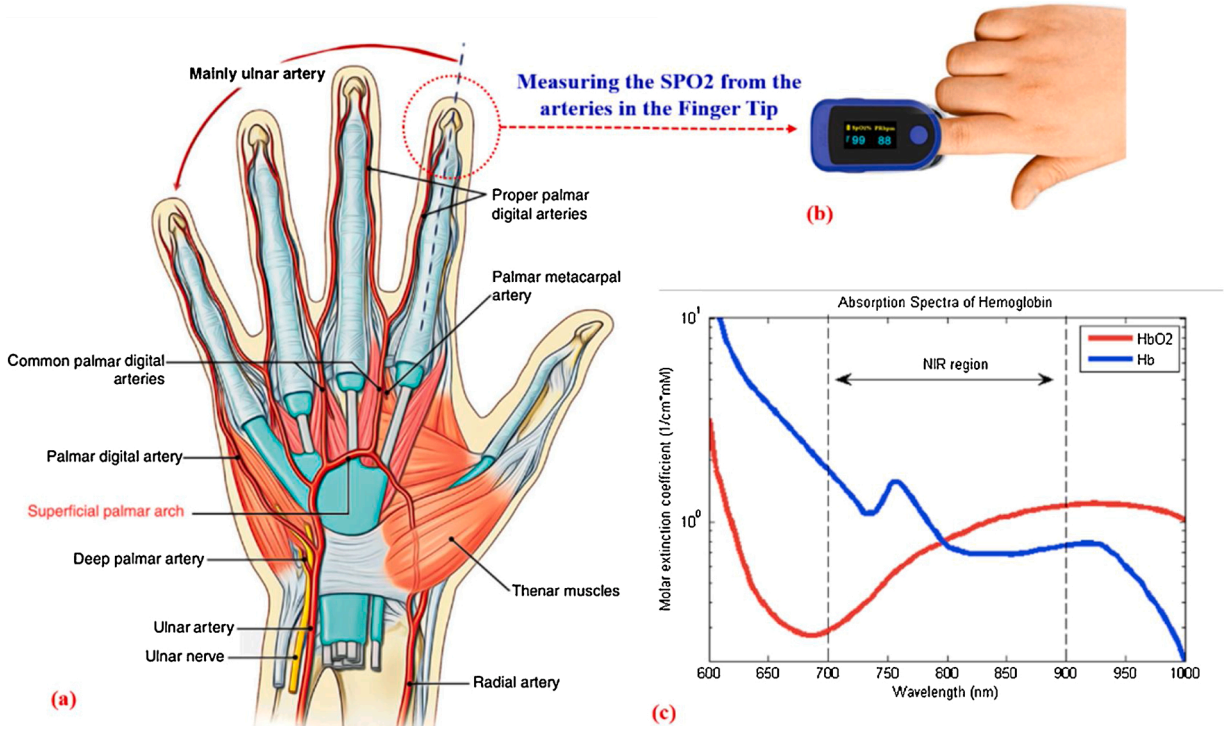

Fig. 1. (a) The Hand Anatomy highlighting the Blood circulation where the (SpO2) measurements in blood from the proper palmer digital arteries demonstrating the optical properties of the oxygenated and de-oxygenated blood through the visible (VIS) and near infra-red (NIR) wavelength, whereby oxygenated hemoglobin absorbs more infrared light and allows more red light to pass through and deoxygenated hemoglobin allows more infrared light to pass through and absorbs more red light; (b) Measuring the oxygen saturation (SPO2) using the Finger Pulse Oximeter (Contec, CMS50D, China); (c) The plot graph for the optical properties of the oxygenated and de-oxygenated blood through the VIS and NIR wavelength.

and trial studies. Conventional observation of SpO2 is applied in arteries as it transports oxygen to the tissues. The gold standard of the non-invasive techniques for SpO2 measurement was known as pulse-oximetry, and it was initially proposed in the 1930s [2,4].

The oxygenated blood (HbO2) and the deoxygenated blood (Hb) molecular configurations lead to different electromagnetic absorption and therefore different emission of light. Pulse-oximetry operates based on this theory of various absorption and light emission [5,6]. The blood circulation of the hand anatomy is shown in Fig. 1a, where the main blood supply is the radial and the ulnar arteries, which ends at the tips of the fingers with the proper palmer digital arteries [6,7]. The pulse oximeter reads the oxygen saturation percentage by applying the finger, as displayed in Fig. 1b.

Although the conventional oximeter utilized two different LED (Red at wavelength 660 nm and NIR at wavelength 940 nm), absorption of light at these wavelengths fluctuates significantly among the blood loaded with oxygen HbO2 and the blood lacking oxygen Hb. However, HbO2 absorbs more infrared light and allows more red light to pass through and Hb allows more infrared light to pass through and absorbs more red light [8–10], as illustrated in Fig. 1c.

Depending upon the optical absorption spectrum of HbO2 and Hb as displayed in Fig. 1c (Figure A1 in the Appendix is additional clarified Figure), it is possible to select two wavelengths, visible- red wavelength range (650 to 700 nm) where Hb is more highly absorbed than HbO2 and the NIR wavelength range 900 to 1000 nm, where the absorbance of HbO2 is higher than Hb.

For accurate measurement, it is preferable that:

1 The measured signals have high SNR at both wavelengths.
2 The optical absorption associated with HbO2 and Hb are opposite and the differences are large at the two wavelengths, as shown in Fig. 1c.

To this point, the traditional contact-based pulse oximetry uses a dual-wavelength LED at red (λ =660 nm) and near infrared (NIR, λ =940 nm) wavelengths as light source, and a photodiode as light detector. The 660 nm and 940 nm wavelength combination produce high quality data for the contact pulse oximetry, but it is not suitable for the suggested noncontact method.

SPO2 has numerous applications in anesthesiology and critical care. Although pulse oximetry is considered sufficiently accurate for many clinical purposes, there are significant limitations (physiological and technical) [11], such as:

1 It needs to be in contact with the patients (finger / ear) [4,11].
2 It is unreliable when peripheral arterial pulsations are reduced (e.g., hypothermia) [12].
3 It is unreliable for patients undergoing prolonged procedures such as cardiac, vascular, reconstructive, or neuro-surgery [13,14].
4 Its response time is about 30 seconds on the finger [15].
5 There are errors in the pulse oximeter readings due to false absorption of carboxyhemoglobin (COHb) and methemoglobin (MetHb) [16–18].
6 Most of the device's accuracy fluctuates by 2 to 3% in the O_2 saturation range of 70-100% [11,19].

Recently, many different methods of measuring (SpO2) appeared such as: Near-Infrared Spectroscopy [20], magnetic resonance imaging (MRI) [21], blood gas analysis [22], transcutaneous oxygen measurement [23], and electron paramagnetic resonance [24]. Each of these strategies has its advantages and restrictions, as far as precision, resolution, time consumption, cost, and so on. More recently, hyperspectral imaging systems (HSI) have demonstrated their incentive to survey tissue oxygenation [25–27].

Nevertheless, the scanned area with the hyperspectral camera for the investigated area between the wrist and the forearm, Region of interest

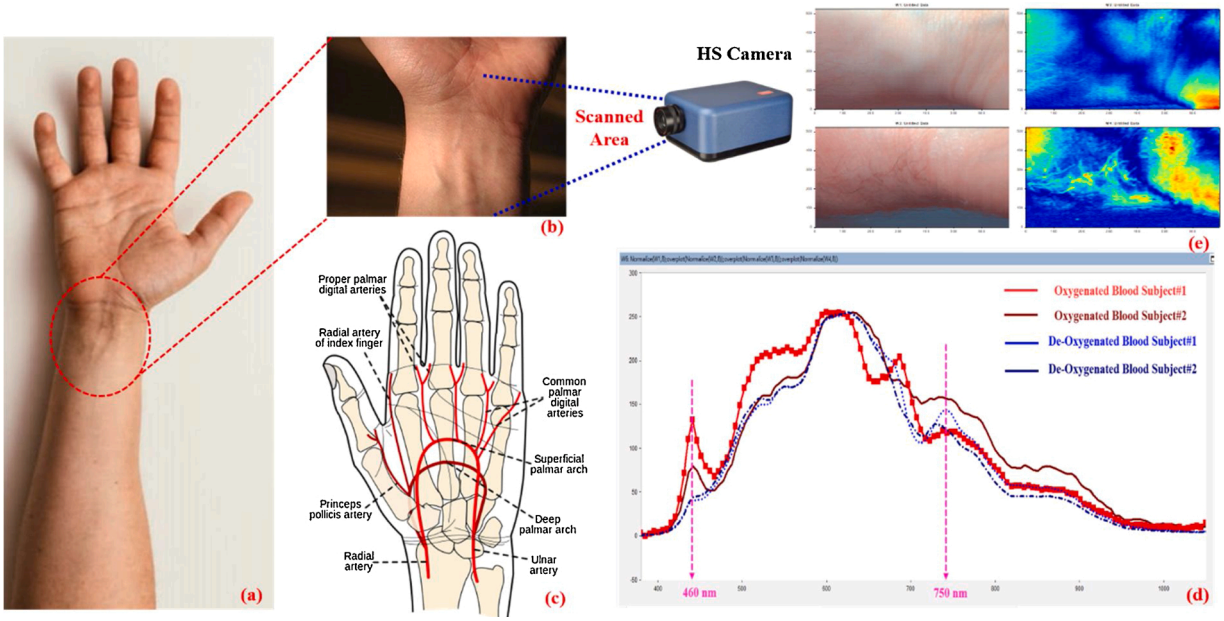

Fig. 2. (a) The forearm is the region of the upper limb between the elbow and the wrist; (b) The Region of interest (ROI) in the investigation trial was scanned area between the forearm and the wrist to highlight its Blood Circulation; (c) The ulnar artery is the main blood vessel with oxygenated blood, of the medial aspects of the forearm. It arises from the brachial artery and terminates in the superficial palmar arch, which joins with the superficial branch of the radial artery; (d) The normalization of the recorded signal signature of the oxygenated and de-oxygenated blood vessels or subject#1 and subject#2; (e) The RGB image of subject#1 and after applying the custom algorithm to highlight the de-oxygenated veins; subject#2 and after applying the custom algorithm to highlight the oxygenated arteries.

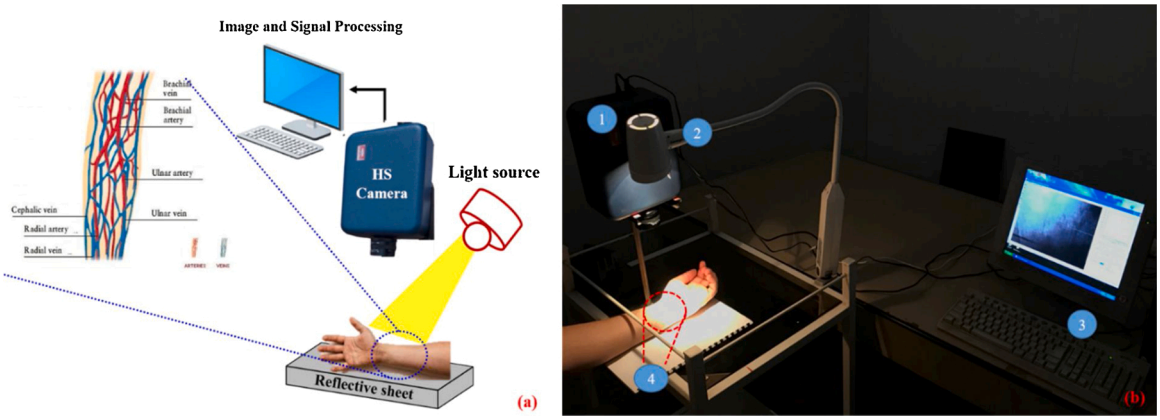

Fig. 3. (a) The Experimental schematic layout demonstrating the main elements of the optical imaging system highlighting the blood circulation for the ROI in the investigated scanned area of the forearm; (b) The actual experimental setup, (1) Hyperspectral Camera (Surface Optics, SOC710, USA), (2) The polychromatic light source (Derungs, 20 P SX, 20 Watt) with a spectral range of 348 to 950 nm, (3) The computer with image and signal preprocessing, (4) The ROI of the investigated forearm of the participants highlighting the scanned area.

(ROI) was highlighted in Fig. 2. This area is considered to be vital as it had both the ulnar and radial arteries (main blood vessel with oxygenated blood) and the ulnar and radial veins (main blood vessel with de-oxygenated blood).

In this present study, we propose a non-contact optical imaging system for mapping the blood circulation under the skin regarding its oxygen concentration, exploiting the HS camera capabilities concerning the conventional methods (SpO2) for COVID-19 pandemic situation, associated with custom algorithm comprising normalization and moving average filtering for noise removal, followed by K-mean clustering for image segmentation to visualize and highlight the arteries and veins in the investigated forearm, in order to assist in phlebotomy, thus estimating the oxygen saturation by taking the ratio between oxygenated arteries and de-oxygenated veins.

2. Materials and Methods

2.1. The main framework protocol

- Sample analysis and data recording for the volunteers.
- Acquiring of the HS Images for the investigated subjects.
- Procedure analysis and image processing.
- Measurements of sample diffuse reflection.
- Delineation of the oxygenated arteries and de-oxygenated veins

2.2. The Trial Procedure

Before this experimental trial, the endorsement was approved by the Institution "*College of Medicine, Ain Shams University; Cairo; EGYPT*" of Ethics Committee, and a written informed consent was given by participants, namely 15 healthy adult patients with mean age 30 years

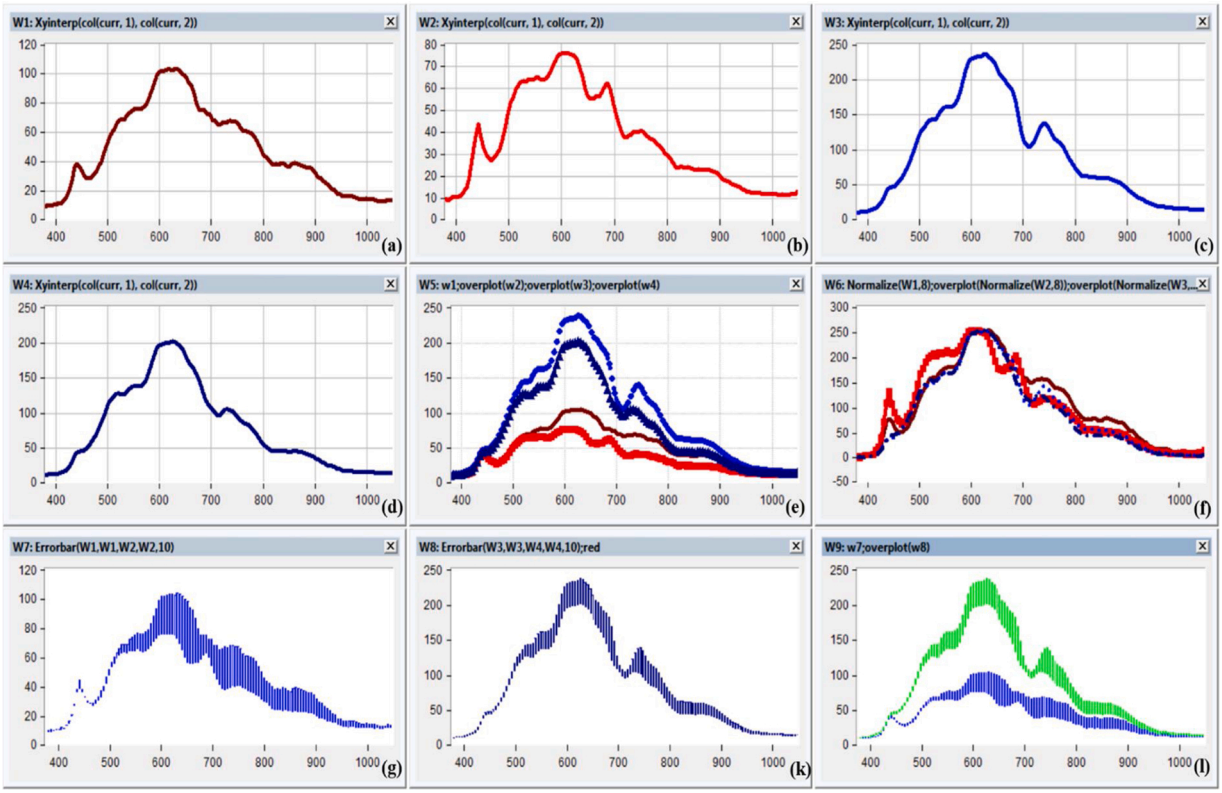

Fig. 4. (a) The signature of the oxygenated arteries of Subject#1 over the spectrum wavelength; (b) The signature of the oxygenated arteries of subject#2 over the spectrum wavelength; (c) The signature of the de-oxygenated veins of subject#1 over the spectrum wavelength; (d) The signature of the de-oxygenated veins of Subject#2 over the spectrum wavelength; (e) The combination of the signal signatures to subject#1 and subject#2; (f) The normalization of the signal signature; (g) The average error intensity for the signature of the oxygenated arteries; (k) The average error intensity for the signature of the de-oxygenated veins; (l) The combination of the signal signatures to the average error intensity for both oxygenated arteries and de-oxygenated veins.

(range 20 to 38 years) who were undergoing phlebotomy and were recruited for this investigation. Participants who suffer from cardiac, respiratory, and peripheral vascular disease were excluded.

The main principle of the custom optical imaging system is more precisely illustrated in Fig. 3, where, the key element to acquire the necessary cube images was a hyperspectral (HS) Camera (Surface Optics, SOC710, USA) with a spectral range of 400 to 1000 nm, a 4.68-nm spectral resolution, and 128 spectral bands. The camera was combined with a lens (Schneider, 1.9/35 CCTV, 400~1000 nm, Germany). The optical setup was aligned and fixed during all the experimental trial, where the departure between the focal point and the investigated samples were kept steady at a distance of 20 cm from the camera setup, the schematic layout of the proposed system is displayed in Fig. 3a.

The scanned area with the hyperspectral camera was the area between the wrist and the forearm, called the Region of interest (ROI), as highlighted in Fig. 3b. This area is considered to be vital, as it embraces the ulnar and radial arteries (main blood vessel with oxygenated blood) and the ulnar and radial veins (main blood vessel with de-oxygenated blood). The regions for the readings were selected according to the vascular locations, according to the medical references.

The main theory of optical imaging for blood oxygen saturation (SpO2) is concisely assessed here. There are three different light interactions from exposing light to the tissue (specular reflection / diffuse reflection / scattering reflection) [28–31].

The investigated trials were conducted on the ROI of the right forearm of 15 healthy male volunteers (range 20 to 38 years) with various skin colors to estimate oxygen saturation by taking the ratio between oxygenated arteries and de-oxygenated veins. For every subject, a two cube image was consecutively captured from each subject for the same skin spot. After image capturing utilizing the HS camera for all the subjects, we applied RGB-IR image segmentation for the region of the interest (ROI) to highlight the oxygenated arteries and de-oxygenated veins (Figure A2 in the Appendix displays the actual setup for the proposed imaging system identifying the ROI).

To validate the captured data of the oxygenated arteries and de-oxygenated veins regarding conventional pulse oximeter measurements, we utilize two different devices (Patient monitor, MEK, MP500, Korea) and (Pulse finger, Contec, CMS50D, China). Both devices were calibrated for quality assurance before the investigation (Figure A3 in the Appendix displays Actual experimental Setup measuring the SPO2).

After capturing the image of the subjects with the HS camera, we measured the diffuse reflectance regarding the various wavelength to select the optimum signature for the oxygenated arteries and the de-oxygenated veins.

After selecting the optimum wavelength to highlight the oxygenated arteries (460 nm) and the de-oxygenated veins (750 nm) we used moving average filtering for noise removal and image enhancement. Finally, we applied K-mean clustering to the optimum wavelength images (460, 750 nm) to delineate the oxygenated arteries and the de-oxygenated veins, respectively.

2.3. *The Custom Algorithm Process*

We built a custom algorithm to measure the optical properties (reflection and attenuation absorption) for the investigated subjects for the sake of HSI calibration, and we employed advanced image procurement for data normalization. Two different captured images for a highly reflected (white cube) and total opaque (dark cube) were used [32]. The basic purpose was to eliminate artifacts and noise impacts on the investigated sample tissue, as given by equation (1):

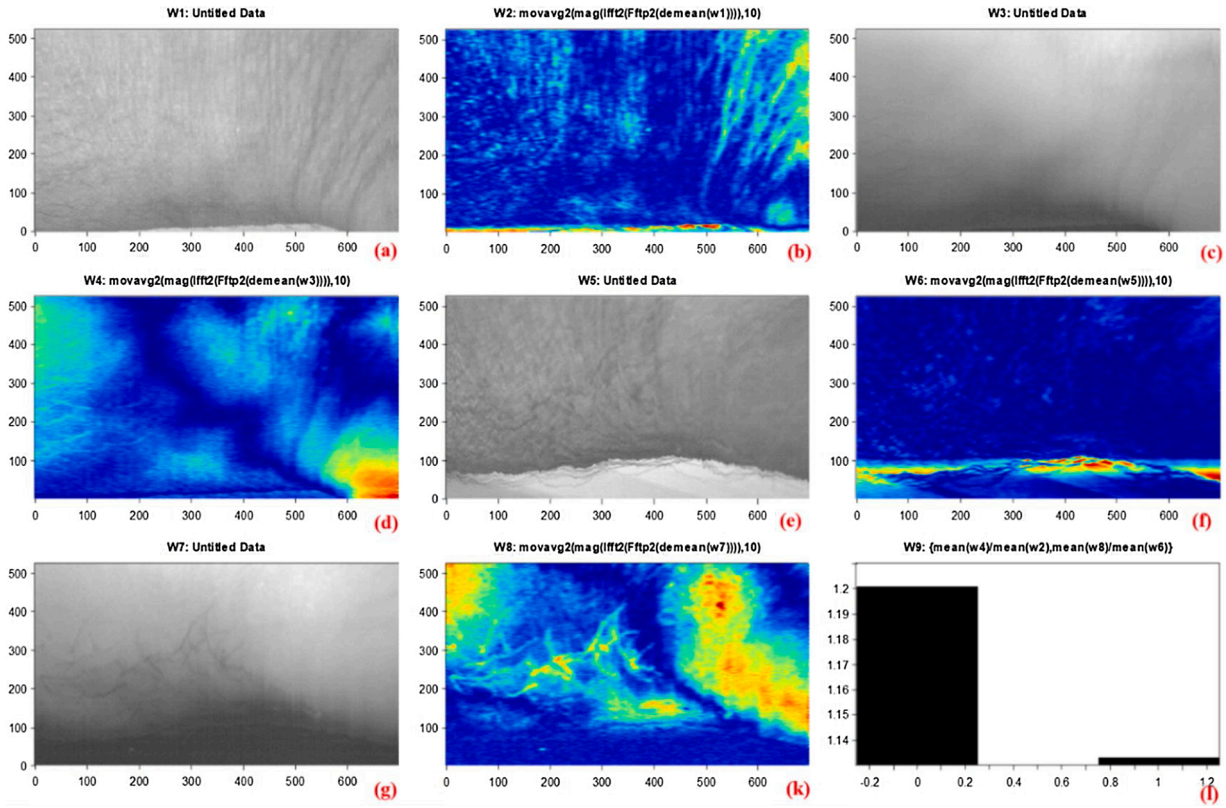

Fig. 5. (a) The HS image of Subject#1 at wavelength 460 nm; (b) Image after applying the custom algorithm to highlight and delineate the oxygenated arteries; (c) The HS image of Subject#1 at wavelength 750 nm; (d) Image after applying the custom algorithm to highlight and delineate the de-oxygenated veins; (e) The HS image of Subject#2 at wavelength 460 nm; (f) Image after applying the custom algorithm to highlight and delineate the oxygenated arteries; (g) The HS image of Subject#2 at wavelength 750 nm; (k) Image after applying the custom algorithm to highlight and delineate the de-oxygenated veins; (l) Bar graph to highlight the difference ratio between the two subject oxygenated arteries and de-oxygenated veins.

$$\text{Ŗ}(\vartheta) = \frac{\tilde{\text{I}}_m(\Phi) - \tilde{\text{I}}_d(\Phi)}{\tilde{\text{I}}_w(\Phi) - \tilde{\text{I}}_d(\Phi)} \times 100\% \tag{1}$$

Where, $\text{Ŗ}(\vartheta)$ is the reflectance of the subject image, $\tilde{\text{I}}_m(\Phi)$ is the acquired image, $\tilde{\text{I}}_d(\Phi)$ is the dark cube image by closing the lens cap, and $\tilde{\text{I}}_w(\Phi)$ is the white cube image.

After applying normalization to the acquired image to eliminate the unwanted spectral impact from the source polychromatic light we employed moving average filtering (K = 10), followed by K-mean image segmentation (K = 8). The corresponding equations are better outlined in previous studies [33,34].

Every collected image by the HS camera was exploited to calculate the light attenuation absorption for each wavelength as shown in equation (2):

$$\tilde{\text{A}} = \log\left(\frac{\ddot{\text{I}}_w}{\ddot{\text{I}}_s}\right) \tag{2}$$

Where, $(\tilde{\text{A}})$ the light attenuation absorption, $(\ddot{\text{I}}_s)$ is the reflected light intensity of the subject hand, $(\ddot{\text{I}}_w)$ is the reflected light intensity from the white reference.

We determined the light attenuation absorption (stated in arbitrary units) of the biological tissue utilizing the modified Beer-Lambert law, as displayed in equation (3):

$$\tilde{\text{A}}(\mathscr{X}, \mathscr{Y}, \omega) = -\log_{10}\left[\frac{\tilde{\text{I}}_t(\mathscr{X}, \mathscr{Y}, \omega) - b(\mathscr{X}, \mathscr{Y}, \omega)}{\tilde{\text{I}}_c(\mathscr{X}, \mathscr{Y}, \omega) - b(\mathscr{X}, \mathscr{Y}, \omega)}\right] \tag{3}$$

Where, $(\mathscr{X}, \mathscr{Y})$ are the spatial pixel coordinates, (ω) is the spectral coordinate (wavelength), $\tilde{\text{I}}_t(\mathscr{X}, \mathscr{Y}, \omega)$ is the HS image of the complete forehand subject, $b(\mathscr{X}, \mathscr{Y}, \omega)$ is the HS image of the ROI to highlight the oxygenated arteries and de-oxygenated veins, $\tilde{\text{I}}_c(\mathscr{X}, \mathscr{Y}, \omega)$ is the reference HS image.

The expectation of the essential health parameter quantity is through the wavelength (ω), dependent light diffusion calculation model defined in equation (4) [35]:

$$\tilde{\text{A}}(\omega) = \sqrt{\frac{3\mu_a(\omega)}{\mu_s(\omega)}} \tag{4}$$

Where, $\mu_a(\omega)$ is the absorption coefficient, $\mu_s(\omega)$ is the reduced scattering coefficient. Moreover, the correlation between the light absorption $\tilde{\text{A}}(\omega)$, and oxygen saturation (SpO2), is provided by equation (5):

$$\mu_a(\omega) = (\,(\dot{\varepsilon}_{HBO2} - \dot{\varepsilon}_{HB})\text{SpO2} + \dot{\varepsilon}_{HB}\,)\text{Ť} \tag{5}$$

Where, $\mu_a(\omega)$ is the absorption coefficient, $(\dot{\varepsilon}_{HBO2})$ the hemoglobin components in the oxygenated blood arteries, $(\dot{\varepsilon}_{HB})$ the hemoglobin components in the de-oxygenated blood veins , (SpO2) is the blood oxygen saturation.

Finally, the contour delineation of the oxygenated arteries and the de-oxygenated veins was overlaid on the images with wavelengths (460 nm, 750 nm), respectively.

3. Results

The participating subject`s forearm was illuminated with the polychromatic source light (348 to 950 nm). The measured diffused reflectance intensity of the ROI by the hyperspectral camera varied regarding the variation of the oxygen blood level. Two of the subject's recorded data were displayed in Fig. 4. The selective regions to extract the

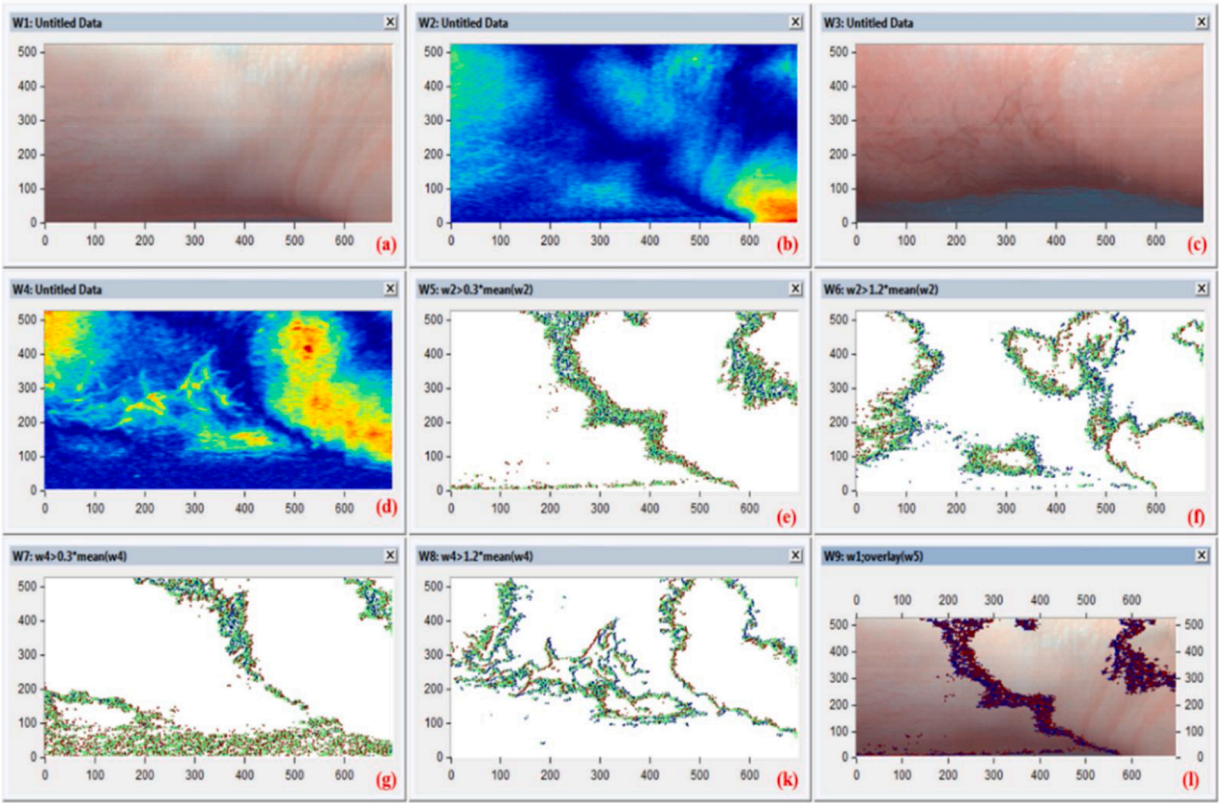

Fig. 6. (a) RGB image of subject#1 ; (b) Image after applying the custom algorithm to highlight and delineate the de-oxygenated veins; (c) The RGB image of subject#2; (d) Image after applying the custom algorithm to highlight and delineate the oxygenated arteries; (e) Applying K-mean clustering with threshold value ≥ 0.3 of the applied window #2 for the veins delineation; (f) Image after applying K-mean clustering with threshold value ≥ 1.2 of the applied window #2 for the veins delineation; (g) Image after applying the K-mean clustering with threshold value ≥ 0.3 of the applied window #4 for the arteries delineation; (k) Image after applying K-mean clustering with threshold value ≥ 1.2 of the applied window #4 for the arteries delineation; (l) The RGB image after final contour mapping to the de-oxygenated veins.

spectral regions for each blood vessel in the ROI were more visualized in the actual setup which was displayed in the methods section and the Appendix.

Notice that Fig. 4a, and b represents the spectral signature of the oxygenated arteries and Fig. 4c, and d represents the de-oxygenated the spectral signature of the veins of Subject#1 and Subject#2, respectively. Fig. 4e displays the combined signal signatures for the two subjects between the oxygenated arteries and the de-oxygenated veins. Next, we applied normalization to these signals, as displayed in Fig. 4f to cancel out the intensity artifact and focus on the variation of the difference spectral signature between the oxygenated and the de-oxygenated areas regarding the spectrum wavelength. Fig. 4l displays the combination of the signal signatures to the average error intensity for both oxygenated arteries and de-oxygenated veins (*Additional clear image for* Fig. 4l *is added in the Appendix as* Figure A5).

After signal normalization we only consider the amplitude intensity variation with the wavelength. At this point we noticed that after capturing the HS image of the subject to select the optimum wavelength to highlight the oxygenated arteries from the de-oxygenated veins through the guidance spectral signature, as shown in Fig. 4f (Figure is enlarged and more clarified as Figure A4 in the Appendix), the oxygenated arteries at wavelength 460 nm were of higher amplitude than the de-oxygenated veins, while at wavelength 750 nm the de-oxygenated veins were of higher amplitude than the oxygenated arteries. Thus, the ideal wavelength to reveal the oxygenated arteries is at wavelength 460 nm and the de-oxygenated veins at wavelength 750 nm.

Then we applied the custom algorithm (normalization and moving average filtering) to highlight and delineate the oxygenated arteries after selecting the optimum wavelength 460 nm. To delineate the de-oxygenated veins, we selected the HS image at wavelength 750 nm and applied the custom algorithm, as displayed in Fig. 5.

We applied the same algorithm to the RGB image of subject#1 and subject#2 using the K-means clustering to delineate the oxygenated arteries and the de-oxygenated veins overlaid on the RGB image, as better shown in Fig. 6.

4. Discussion

The oxygen saturation in the blood (SpO2) is a significant factor for clinical diagnosis, such as hypoxemia, sepsis, or decompression sickness [2]. Additionally, The degree of the oxygen level in the blood can be exploited as an observation parameter for cardiac and respiratory system illness, diabetic ulcers in the foot, plastic surgeries, and burned skin [1].

The HS image capture time was in the range of 3 to 6 sec, and the image processing time was less than 10 sec utilizing a DADiSP/SE image analysis software (DSP Development Corporation, 6.7 student edition, 2020), on a laptop with processor (Intel core i7 @1.8 GHz and a 16 GB RAM). Finally, the entire process takes about 13 to 16 sec to identify the oxygenated and the de-oxygenated blood vessels and to calculate the percentage oxygen saturation.

We used Fig. 4 as a guidance to identify the spectral signature of the oxygenated arteries and the de-oxygenated veins, whereas Fig. 4e displays the combination of the signal signatures to Subject#1 and Subject#2 regarding the intensity. Then we applied normalization in Fig. 4f to remove the intensity artifact and focus on the variation of the difference signature between the oxygenated and the de-oxygenated regarding the spectrum wavelength only.

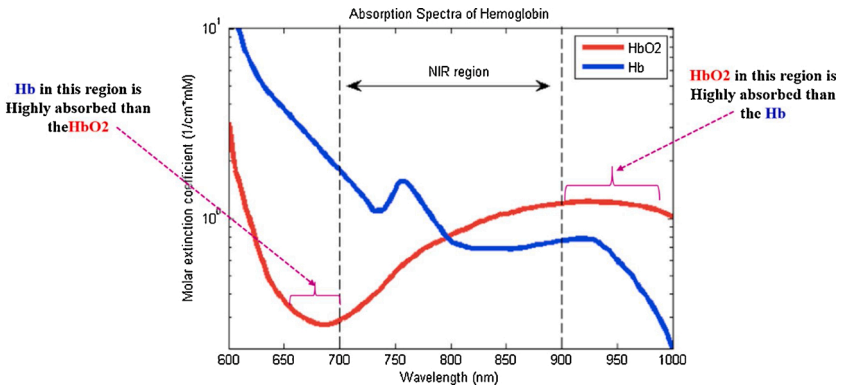

Fig. A1. explains the visible- red wavelength range (650 to 700 nm) where Hb is more highly absorbed than HbO2 and NIR wavelength range (900 to 1000 nm), where the absorbance of HbO2 is more than Hb.

By focusing on Fig. 4f (*Additional clear image for* Fig. 4*f is added in the Appendix as Figure* A4), we neglect the amplitude of the intensity and consider the variation with the spectral wavelength only. We notice that at wavelength 460 nm the oxygenated arteries were of higher intensity than the de-oxygenated veins and at wavelength 750 nm the de-oxygenated veins were of higher intensity than the oxygenated arteries. Thus, the ideal wavelength to reveal the oxygenated arteries is 460 nm, and the ideal wavelength to reveal de-oxygenated is 750 nm.

We applied the custom algorithm (normalization and moving average filtering) to the spectral images to highlight and delineate the oxygenated arteries after selecting the optimum wavelength (460 nm) for Subject#1, as shown in Fig. 5a (before algorithm application) and Fig. 5b (following algorithm application). To delineate the de-oxygenated veins, we selected the HS image at wavelength 750 nm for Subject#2 and applying the custom algorithm, as displayed in Fig. 5c and Fig. 5d (similar to Fig. 5a and b, respectively). We repeated the same steps for Subject#2, as clarified in Fig. 5e, f, g, and k. Finally, the bar graph to highlight the difference ratio between the two subjects' oxygenated arteries and de-oxygenated veins is shown in Fig. 5l.

We repeated the same algorithm with a variable threshold value on the RGB image of Subject#1 and Subject#2 using K-mean clustering to delineate the oxygenated arteries and the de-oxygenated veins overlaid on the RGB image, as better visualized in Fig. 6 (*more additional illustration images were added in the Appendix as* Figure A6 *and* Figure A7).

5. Conclusion

The presented results of the proposed prospective system can provide precise information for a real-time, non-contact oxygen saturation approach. This innovation may likewise broaden the advantages of cutting-edge SPO2 monitoring to more extensive patient populations to assist with phlebotomy and vascular research. Additionally, they may permit future surgical or pharmacological intersessions that titrate or limit ischemic injury continuously.

It is true that a hyperspectral camera is usually very expensive indeed and not easy to work directly on the captured image cube, which needs to be processed with another software program. That is why our goal was to use the HS camera initially to select the optimum wavelength to highlight the oxygenated and the de-oxygenated blood vessels, then to use the commercial camera with the optical filter in the future.

In the end, we conclude that HS optical imaging system will be able to avoid many constraints regarding the conventional SPO2, such as:

1 Being a non-contact system there is no need to measure from the patients (finger / ear), especially in view of the pandemic situation of COVID-19.
2 Its ability to identify remotely the oxygenated and de-oxygenated blood vessels to measure the oxygen saturation.

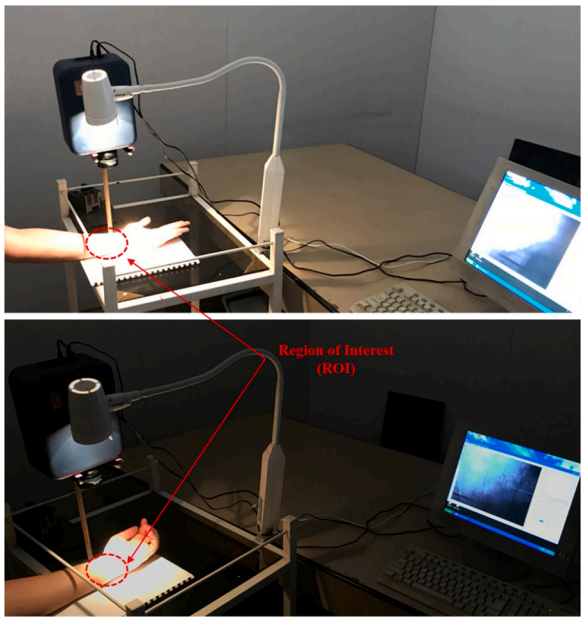

Fig. A2. The actual setup for the proposed optical imaging system identifying the Region of interest (ROI) to highlight the oxygenated blood and the de-oxygenated blood.

3 Its tremendous reliability under several clinical conditions such as cardiac, vascular, or neuro-surgical conditions.
4 Its high reliability at the detection of low peripheral arterial pulsations (hypothermia).
5 Its reasonably short response time (13 to 16 sec).

Funding

The authors state and declare that there are no funders for this study.

Ethics approval

All experimental and investigation trials was approved and validated from "Ain Shams University" – Medical College - Ethics Committee.

Consent to participate

No experimental investigation was performed on individuals within this research study.

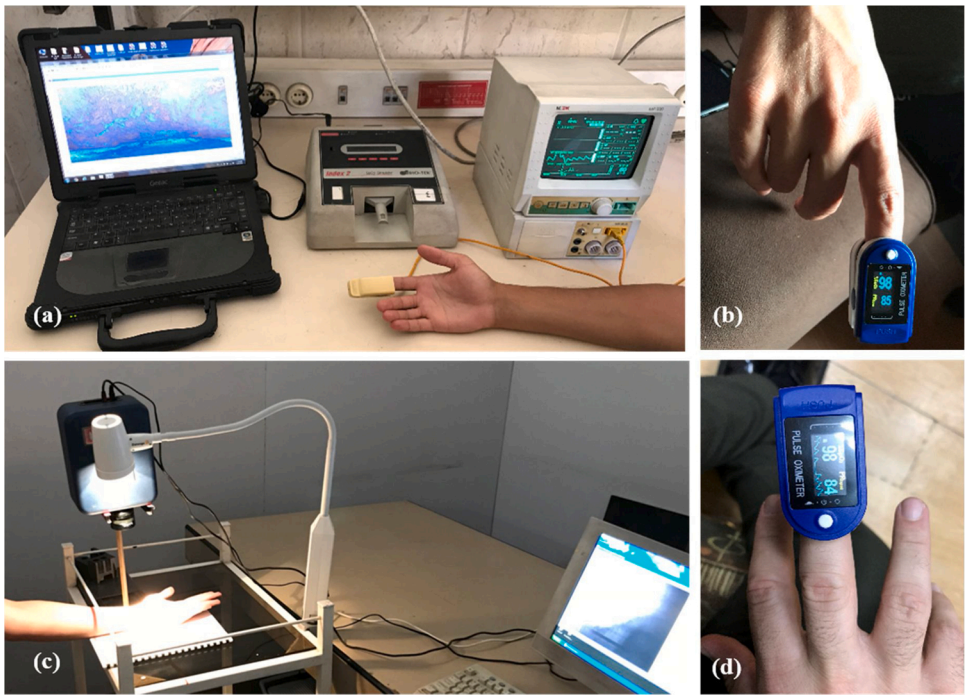

Fig. A3. (a) Actual experimental Setup measuring the oxygen saturation (SPO2) for one of the participating subjects using the Patient monitor (MEK, MP500, Korea) after calibrating it with device (Biotek, Index2, USA); (b) The same subject measuring his (SPO2) with Pulse finger (Contec, CMS50D, China) both two data was recorded applying the mean value to be compared regarding the spectral images; (c) The Custom non-invasive optical imaging system to acquire the spectral images and measuring the diffuse reflectance of each subject ; (d) Measuring the (SPO2) with Pulse finger for another subject.

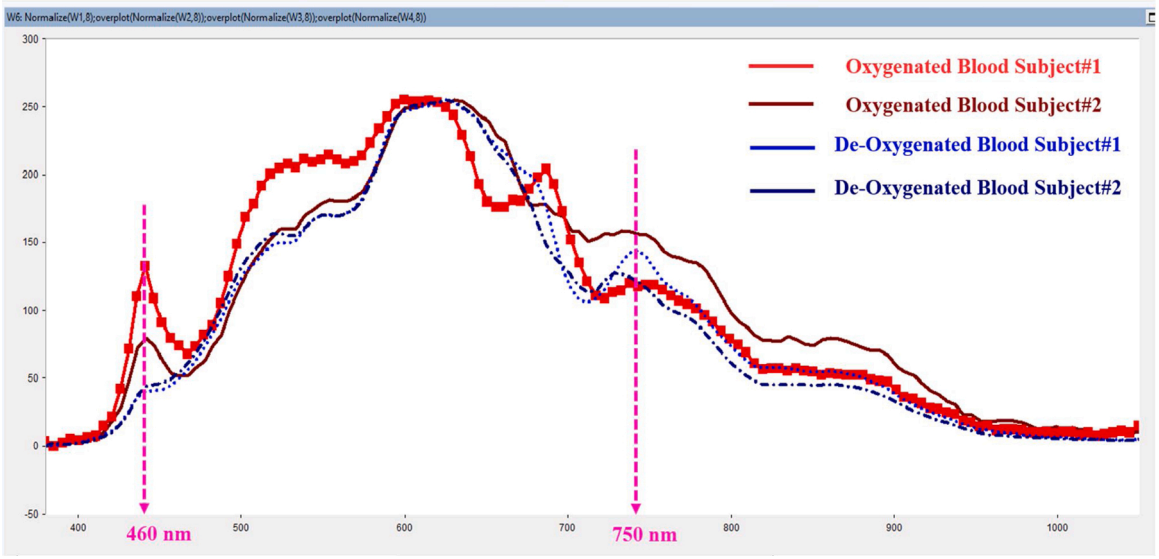

Fig. A4. The normalization of the recorded signal signature of the oxygenated and de-oxygenated blood vessels or subject#1 and subject#2.

Consent for publication

All the co-authors agree upon the research study publication.

Availability of data and material

The authors stated and declare that all data is existing and available.

Code availability

The authors stated and declare that all code is existing and available.

Declaration of Competing Interest

The authors report no declarations of interest.

Appendix A

.

References

[1] S. Miclos, S.V. Parasca, M.A. Calin, D. Savastru, D. Manea, Algorithm for mapping cutaneous tissue oxygen concentration using hyperspectral imaging, Biomed. Opt. Express. 6 (2015) 3420, https://doi.org/10.1364/boe.6.003420.
[2] U. Rubins, A. Grabovskis, J. Cimurs, Z. Marcinkevics, A. Caica, Hyperspectral evaluation of skin blood oxygen saturation at baseline and during arterial occlusion, 2018, p. 42, https://doi.org/10.1117/12.2306131.
[3] H. Zhao, R.H. Webb, B. Ortel, A new approach for noninvasive skin blood imaging in microcirculation, Opt. Laser Technol. 34 (2002) 51–54, https://doi.org/10.1016/S0030-3992(01)00093-7.
[4] M.W. Wukitsch, Pulse oximetry: Historical review and Ohmeda functional analysis, Int. J. Clin. Monit. Comput. 4 (1987) 161–166, https://doi.org/10.1007/BF02915903.

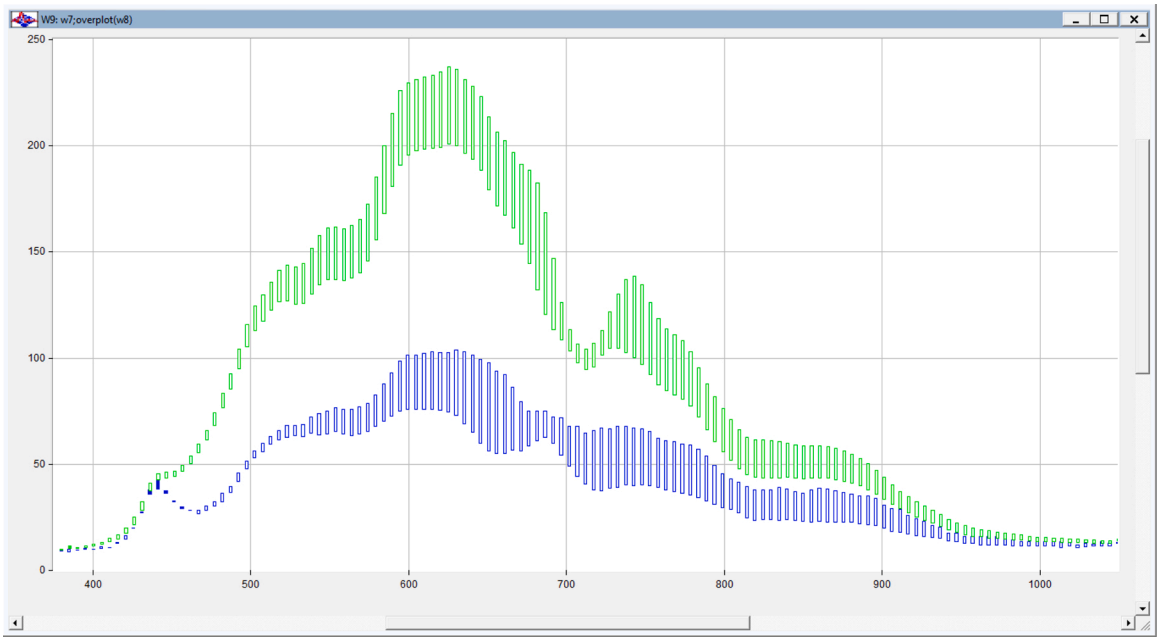

Fig. A5. The combination of the signal signatures to the intensity average error of the intensity for both oxygenated arteries and de-oxygenated veins of two different subjects.

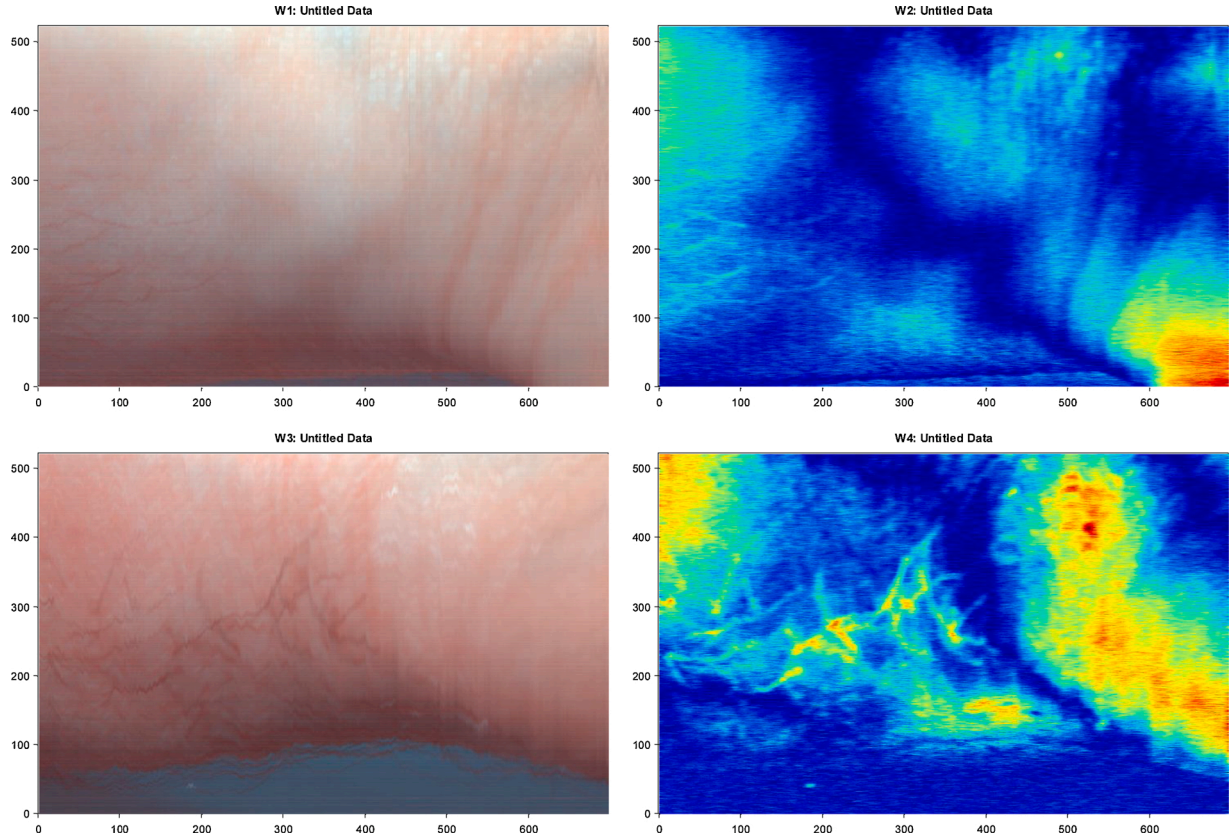

Fig. A6. The RGB image of subject#1 and after applying the custom algorithm to highlight the de-oxygenated veins; subject#2 and after applying the custom algorithm to highlight the oxygenated arteries.

[5] C.J. Blaisdell, S. Goodman, K. Clark, J.F. Casella, G.M. Loughlin, Pulse Oximetry Is a Poor Predictor of Hypoxemia in Stable Children With Sickle Cell Disease, Arch. Pediatr. Adolesc. Med. 154 (2000) 900–903.
[6] A. Jubran, Pulse oximetry, Crit. Care. (2015) 1–7, https://doi.org/10.1186/s13054-015-0984-8.
[7] T. Aoyagi, Improvement of the earpiece oximeter, Abstr. Japanese Soc. Med. Electron. Biol. Eng. 1974 (1974) 90–91.
[8] M.W. Wukitsch, M.T. Petterson, D.R. Tobler, J.A. Pologe, Knowing Your Monitoring Equipment, 1988, pp. 290–301.
[9] G. Zonios, U. Shankar, V.K. Iyer, Pulse Oximetry Theory and Calibration for Low Saturations, IEEE Trans. Biomed. Eng. 51 (2004) 818–822.

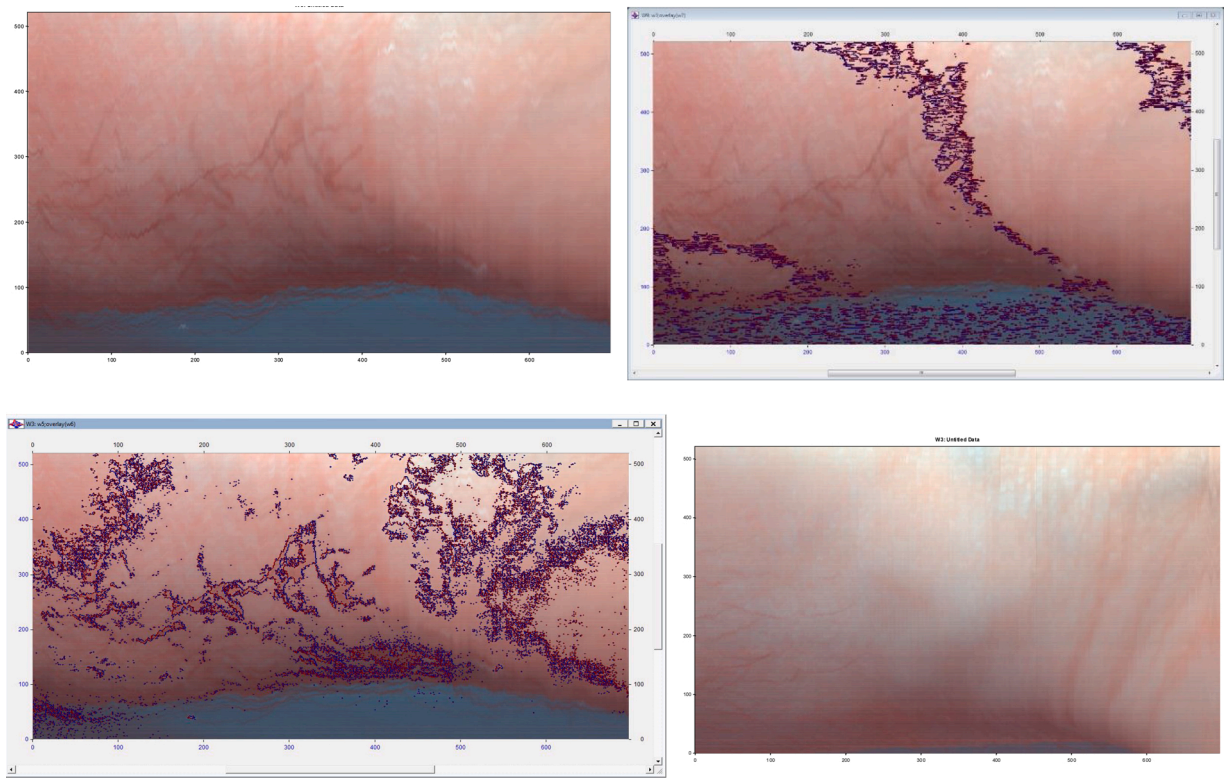

Fig. A7. The RGB image of the investigated subject applying the custom algorithm to highlight the de-oxygenated veins and the oxygenated arteries.

[10] N.K. Corporation, Pulse oximetry : its invention, theory, and future, 2003, pp. 259–266, https://doi.org/10.1007/s00540-003-0192-6.

[11] J.F. Kelleher, in: Joseph F. Kelleher (Ed.), PULSE OXIMETRY, 1989, pp. 37–62. MD.

[12] Y. Shimada, I. Yoshiya, N. Oka, K. Hamaguri, Effects of multiple scattering and peripheral circulation on arterial oxygen saturation measured with a pulse-type oximeter, Med. Biol. Eng. Comput. 22 (1984) 475–478.

[13] A.C. Ralston, R.K. Webb, W.B. Runciman, Potential errors in pulse oximetry III: effects of interference, dyes, dyshaemoglobins and other pigments, Anaesthesia. 46 (1991) 291–295.

[14] D.L. Reich, A. Timcenko, C.A. Bodian, J. Kraidin, J. Hofman, M. DePerio, S. N. Konstadt, T. Kurki, J.B. Eisenkraft, Predictors of pulse oximetry data failure, Anesthesiol. J. Am. Soc. Anesthesiol. 84 (1996) 859–864.

[15] J.G. Webster, Design of pulse oximeters, CRC Press, 1997.

[16] T. Richardson, Methemoglobinemia and pulse oximetry, Respir. Care. 50 (2005) 386.

[17] S.J. Barker, K.K. Tremper, The effect of carbon monoxide inhalation on pulse oximetry and transcutaneous PO2, Anesthesiol. J. Am. Soc. Anesthesiol. 66 (1987) 677–679.

[18] S.J. Barker, K.K. Tremper, J. Hyatt, Effects of methemoglobinemia on pulse oximetry and mixed venous oximetry, Anesthesiol. J. Am. Soc. Anesthesiol. 70 (1989) 112–117.

[19] J.E. Sinex, Pulse oximetry: principles and limitations, Am. J. Emerg. Med. 17 (1999) 59–66.

[20] S. Hyttel-Sorensen, L.C. Sorensen, J. Riera, G. Greisen, Tissue oximetry: a comparison of mean values of regional tissue saturation, reproducibility and dynamic range of four NIRS-instruments on the human forearm, Biomed. Opt. Express. 2 (2011) 3047–3057.

[21] T. Christen, P. Bouzat, N. Pannetier, N. Coquery, A. Moisan, B. Lemasson, S. Thomas, E. Grillon, O. Detante, C. Rémy, Tissue oxygen saturation mapping with magnetic resonance imaging, J. Cereb, Blood Flow Metab. 34 (2014) 1550–1557.

[22] M.D. Davis, B.K. Walsh, S.E. Sittig, R.D. Restrepo, AARC clinical practice guideline: blood gas analysis and hemoximetry: 2013, Respir. Care. 58 (2013) 1694–1703.

[23] S.V.S. Rithalia, Developments in transcutaneous blood gas monitoring: a review, J. Med, Eng. Technol. 15 (1991) 143–153.

[24] H.M. Swartz, N. Khan, J. Buckey, R. Comi, L. Gould, O. Grinberg, A. Hartford, H. Hopf, H. Hou, E. Hug, Clinical applications of EPR: overview and perspectives, NMR Biomed. 17 (2004) 335–351.

[25] G. Lu, B. Fei, Medical hyperspectral imaging: a review, J. Biomed. Opt. 19 (2014) 10901.

[26] D.R. McCormack, A.J. Walsh, W. Sit, C.L. Arteaga, J. Chen, R.S. Cook, M.C. Skala, In vivo hyperspectral imaging of microvessel response to trastuzumab treatment in breast cancer xenografts, Biomed. Opt. Express. 5 (2014) 2247–2261.

[27] M.A. Calin, S.V. Parasca, D. Savastru, D. Manea, Hyperspectral imaging in the medical field: present and future, Appl. Spectrosc. Rev. 49 (2014) 435–447.

[28] A. Rehman, I. Ahmad, K. Rehman, S. Anwar, S. Firdous, M. Nawaz, Optical properties measurement of highly diffusive tissue phantoms for biomedical applications, Laser Phys. 25 (2014) 25605.

[29] M.C. Method, Role of Optical Properties on Photon Distribution in a Biological Tissue Using, J. Sci. Ind. Res. 76 (2017) 154–159.

[30] S.L. Jacques, O. Health, Optical Properties of Biological Tissues : A Review Optical properties of biological tissues : a review, Phys. Med. Biol. (2014), https://doi.org/10.1088/0031-9155/58/11/R37.

[31] V. Tuchin, Tissue Optics, Photonics: Light-Tissue Interaction II, J. Biomed. Photonics Eng. 2 (2016), 030201, https://doi.org/10.18287/jbpe16.02.030201.

[32] S.S.M. Noor, K. Michael, S. Marshall, J. Ren, Hyperspectral image enhancement and mixture deep-learning classification of corneal epithelium injuries, Sensors (Switzerland). 17 (2017), https://doi.org/10.3390/s17112644.

[33] I.H. Aboughaleb, M.H. Aref, Y.H. El-sharkawy, Photodiagnosis and Photodynamic Therapy Hyperspectral imaging for diagnosis and detection of ex-vivo breast cancer, Photodiagnosis Photodyn. Ther. 31 (2020) 101922, https://doi.org/10.1016/j.pdpdt.2020.101922.

[34] M.H. Aref, Biomedical Research and Clinical Reviews, Biomed. Res. Clin. Rev. 1 (2020) 1–13, https://doi.org/10.31579/brcr.2020/005.

[35] A.K.C. Huong, Spectroscopic analysis of scattering media via different quantification techniques, 2012.